ACS OMEGA

http://pubs.acs.org/journal/acsodf

Article

Double-Layer Solid Composite Electrolytes Enabling Improved Room-Temperature Cycling Performance for High-Voltage Lithium Metal Batteries

Lei Zou, Kun Shi,* Zhengjie Xu, Zeheng Yang, and Weixin Zhang*

Cite This: *ACS Omega* 2022, 7, 994−1002

Read Online

ACCESS | Metrics & More | Article Recommendations | Supporting Information

ABSTRACT: The development of solid-state electrolytes (SSEs) for high energy density lithium metal batteries (LMBs) usually needs to take into account of the interfacial compatibility against lithium metal and the electrolyte stability suitable for a high-potential cathode. In this study, through a facile two-step coating process, novel double-layer solid composite electrolytes (SCEs) with Janus characteristics are customized for the high-voltage LMBs with improved room-temperature cycling performance. Among which, high-voltage resistant poly(vinylidene fluoride) (PVDF) is adopted here for the construction of an electrolyte layer facing the cathode, while the other layer against the lithium anode is composed of the polymer matrix of poly(ethylene oxide) (PEO) blended with PVDF to obtain a lithium metal-friendly interface. With the further incorporation of Laponite clay, the PVDF/(PEO+PVDF)-L SCEs not only exhibit improved mechanical properties, but also achieve a highly increased ionic conductivity (5.2×10^{-4} S cm^{-1}) and lithium ion migration number (0.471) at room temperature. The assembled NCM523|PVDF/(PEO+PVDF)-L SCEs|Li cells thus are able to deliver the initial discharge capacity of 153.9 mAh g^{-1} with 80.8% capacity retention after 200 cycles at 0.3 C. Such easily manufactured double-layer SCEs capable of operating steadily at room temperature provide a competitive electrolyte option for high-voltage solid-state LMBs.

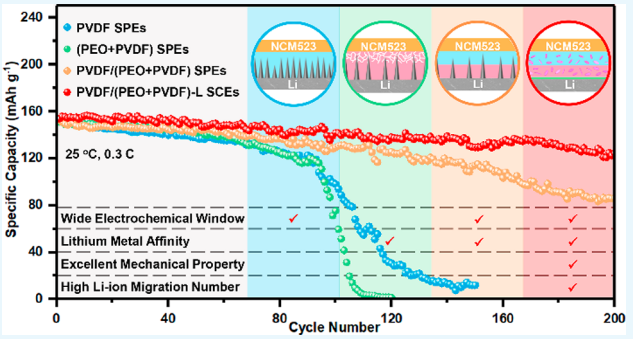

INTRODUCTION

Relying on the extremely high theoretical specific capacity (3860 mAh g^{-1}) and ultralow potential (−3.04 V vs standard hydrogen electrode) of lithium metal anodes, lithium metal batteries (LMBs) have been expected to be one of the most promising energy storage devices with high energy density.[1−4] On the one hand, however, an unstable solid electrolyte interface (SEI) often forms in conventional LMBs owing to the heterogeneous lithium deposition and natural reaction between liquid electrolyte and lithium metal,[5,6] which seriously hinders the exertion of battery capacity or even causes a battery short circuit due to the accompanying uncontrolled lithium dendrite growth.[7,8] On the other hand, to maximize the energy density of batteries, lithium metal anodes need to be matched with high-voltage cathodes, and it thus puts forward urgent demands for more stable electrolytes enabling sustained high voltage. To solve these issues, various strategies have been explored, such as constructing artificial SEI layers,[9−11] adding electrolyte fillers,[12−14] replacing the liquid electrolyte with solid-state electrolytes (SSEs),[15−17] and so on.[18,19] Among them, introducing SSEs into LMBs has received the most attention due to their high safety and effective lithium dendrite inhibition.[20] Accordingly, developing the SSEs with excellent interfacial compatibility to lithium metal anodes as well as high-voltage stability to cathodes for high-performance LMBs becomes particularly critical and is of great significance.

Generally, SSEs include solid inorganic electrolytes (SIEs), solid polymer electrolytes (SPEs), and solid composite electrolytes (SCEs).[21] SIEs have attracted attention mainly because of their high ionic conductivity and large moduli for lithium dendrite inhibition, but their inherent mechanical brittleness and high interface impedance leads to severely limited utilization.[21−23] Compared with SIEs, SPEs are known for the easier processing, higher mechanical flexibility, and better interfacial compatibility, while they always show a low ionic conductivity at 25 °C (<10^{-4} S cm^{-1}), which is hard to meet the normal operation of room-temperature batteries.[21,24,25] As a solution to the issues, SCEs constructed through compounding inorganic fillers with SPEs are considered to be the most promising candidate for safe electrolytes on account of the combined advanced features of

Received: October 6, 2021
Accepted: November 30, 2021
Published: December 21, 2021

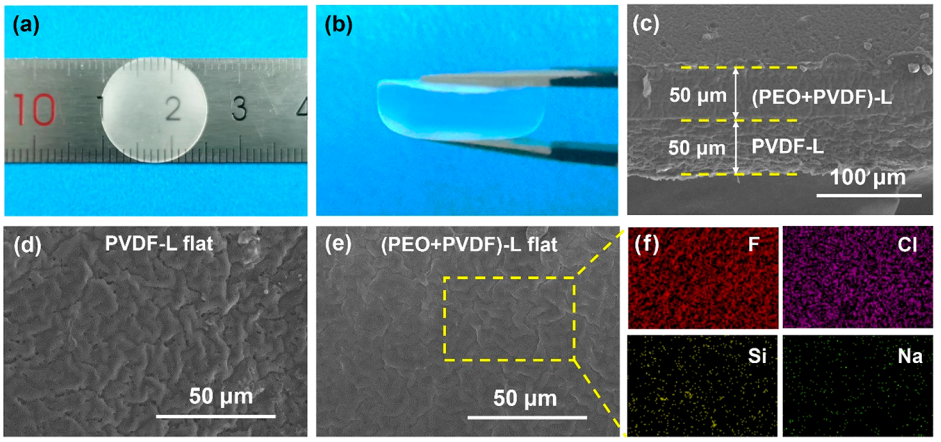

Figure 1. (a, b) Optical photographs and (c) cross-sectional FESEM image of the PVDF/(PEO+PVDF)-L SCEs. (d,e) Surface FESEM images of (d) PVDF-L and (e) (PEO+PVDF)-L flats. (f) EDS mapping of PVDF/(PEO+PVDF)-L for the elements of F, Cl, Si, and Na.

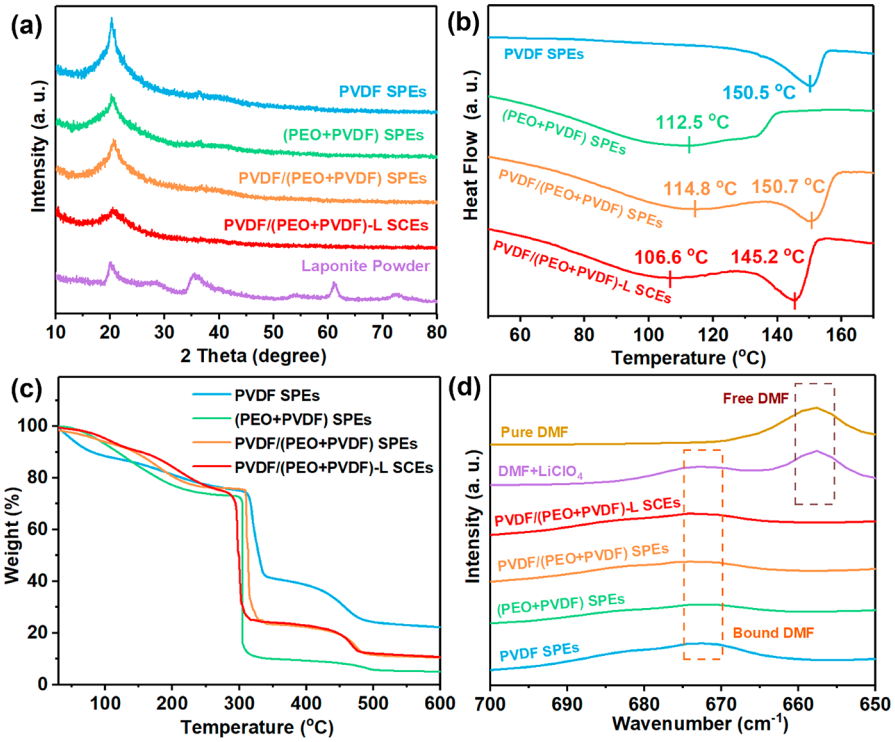

Figure 2. (a) XRD patterns, (b) DSC profiles, (c) TGA curves, and (d) FTIR spectra of the as-prepared PVDF/(PEO+PVDF)-L SCEs and control groups.

SIEs and SPEs, such as acceptable ionic conductivity, good interface contact with electrodes, improved mechanical strength to realize lithium dendrite inhibition, and so on.[26−29] Unfortunately, a monocomponent polymer matrix for SCEs is still powerless to satisfy the increasingly diversified demands.

For instance, as one of the most extensively researched polymer electrolyte substrates, poly(ethylene oxide) (PEO) possesses excellent stability to the lithium metal anodes with low potential as well as fine interface contact with the electrodes owing to the soft texture,[28,29] but it shows poor mechanical property when mixed with high-content lithium salt, and more seriously, it suffers gradual oxidation or decomposition once matched with high-voltage cathodes (>3.9 V).[29,30] By contrast, poly(vinylidene fluoride) (PVDF) that is also employed as a common polymer electrolyte material can exhibit a wide electrochemical window enabling constant high voltage due to the existence of strongly electron withdrawing groups (−C−F),[31] while its interface to lithium metal anodes always appears unstable, resulting in poor cycling performance.[32,33] The promising efforts to overcome such incompatibility between a wide electrochemical window and good interface stability focuses on constructing multilayer SCEs with Janus characteristics.[21,23,28,30,33]

Herein, novel double-layer SCEs consisting of an antioxidative PVDF-based layer facing the cathode and a lithium metal-friendly (PEO+PVDF)-based layer against the anode, are proposed for room-temperature high-voltage LMBs. Specially, the bipolymer feature of the (PEO+PVDF)-based layer therein not only endows the electrolytes with excellent

https://doi.org/10.1021/acsomega.1c05576
ACS Omega 2022, 7, 994−1002

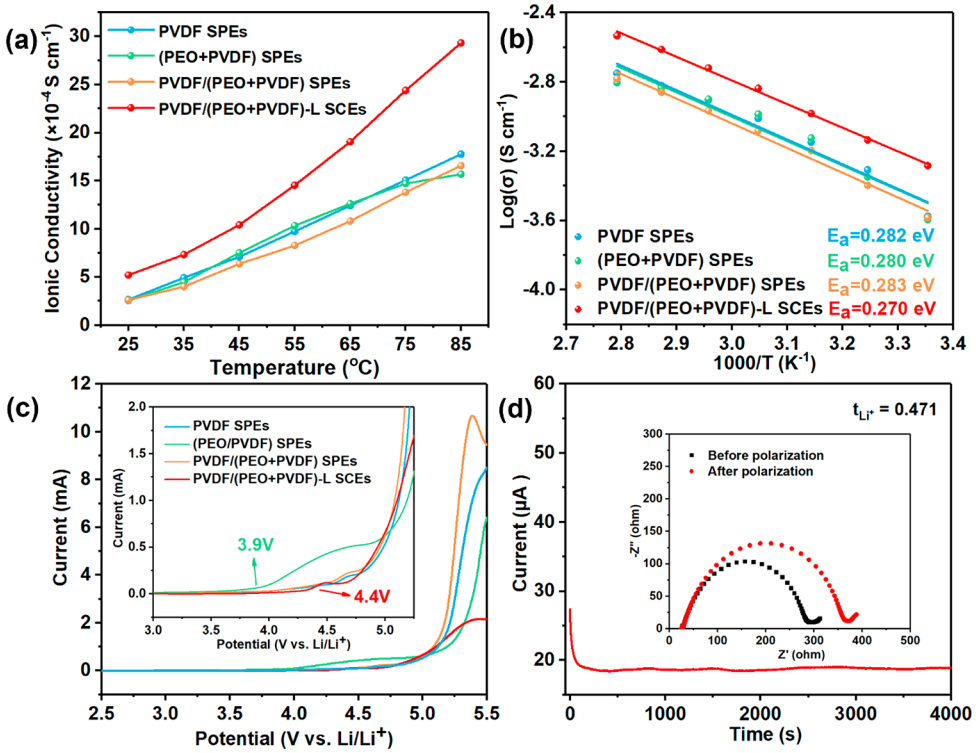

Figure 3. (a) Ionic conductivities, (b) Arrhenius plots, and (c) LSV curves of PVDF/(PEO+PVDF)-L SCEs and the control groups. (d) DC polarization curve for the Li|PVDF/(PEO+PVDF)-L|Li cell under 10 mV. (inset) EIS before and after the polarization.

lithium affinity but also avoids the PEO-introduced mechanical softness with the help of the mechanical support of PVDF polymers. Moreover, laponite clay as an inorganic nanofiller is creatively incorporated into the whole SCE membranes to further improve the mechanical properties for lithium dendrite inhibition as well as realize higher ionic conductivity and larger lithium ion migration number (t_{Li}^{+}). As a result, the SCEs with Janus characteristics (denoted as PVDF/(PEO+PVDF)-L) exhibit the advantages of both a wide electrochemical window and excellent interfacial compatibility to lithium metal; meanwhile, the solid-state LMBs assembled with PVDF/(PEO+PVDF)-L SCEs, high-voltage NCM523 cathodes, and lithium anodes are able to deliver a high specific capacitance and improved cycling and rate performance at room temperature.

RESULT AND DISCUSSION

Micromorphology of PVDF/(PEO+PVDF)-L SCEs. The PVDF/(PEO+PVDF)-L SCEs are prepared through a layer-by-layer coating method to ensure that the internal layers are closely connected (Figure S1). As presented in Figure 1a, the as-prepared PVDF/(PEO+PVDF)-L SCE membrane appears transparent indicating the uniform dispersion of laponite clay nanosheets inside. In addition, a high degree of bending deformation reflects its excellent mechanical flexibility (Figure 1b). The PVDF/(PEO+PVDF)-L SCE membrane exhibits the total thickness of about 100 μm, which is composed of equal thickness PVDF-L and (PEO+PVDF)-L layers closely bonded to each other (Figure 1c). The membrane surface on the PVDF-L side shows a typical rough morphology with visible voids and cracks (Figure 1d),[34] whereas that of the (PEO+PVDF)-L layer displays a relatively smoother flat due to the incorporation of the PEO component (Figure 1e), which can be conducive to improve the contact between the electrolyte membrane and electrode for low interface impedance.[35] In addition, the EDS mapping images confirm that all the components are highly homogeneous, in which "F" represents PVDF, "Cl" indicates $LiClO_4$, while "Si" and "Na" belong to the limited laponite clay (Figure 1f).

Composition Analyses and Physical Properties of PVDF/(PEO+PVDF)-L SCEs. XRD patterns of the as-prepared electrolyte membranes are employed to investigate the composition information (Figure 2a). The high-intensity characteristic peaks at 2θ = 18.5° and 20.1° corresponding to PVDF and that at 2θ = 19.2° and 23.6° belonging to PEO both indicate the high degree of crystallization at ambient temperature.[36] However, only a weakened peak at about 2θ = 20.3° can be found for all the electrolyte membranes, which may be due to the substantial reduction on polymer crystallinity caused by the addition of lithium salt.[36] Among them, with the help of laponite clay, the PVDF/(PEO+PVDF)-L SCEs exhibit the lowest crystallinity with the characteristic peak as the weakest and widest one.[37] Moreover, none of the diffraction peaks representing laponite clay appear in the XRD curve of PVDF/(PEO+PVDF)-L SCEs, suggesting the uniform dispersion of clay nanosheets inside the polymer matrix.

Meanwhile, the crystallinity information on PVDF/(PEO+PVDF)-L SCEs can be accurately reflected by the DSC curves. As presented in Figure 2b, the (PEO+PVDF) SPEs show a much lower melting temperature of 112.5 °C than that of PVDF SPEs (150.5 °C), owing to the natural lower crystallinity of PEO compared to PVDF polymer.[36] As expected, the double-layer PVDF/(PEO+PVDF) SPEs thus possess the combined crystallinity characteristics with the two melting points of 114.8 and 150.7 °C corresponding the (PEO+PVDF) and PVDF components, respectively. Consistent with the XRD results, with the addition of laponite clay, the PVDF/

https://doi.org/10.1021/acsomega.1c05576
ACS Omega 2022, 7, 994−1002

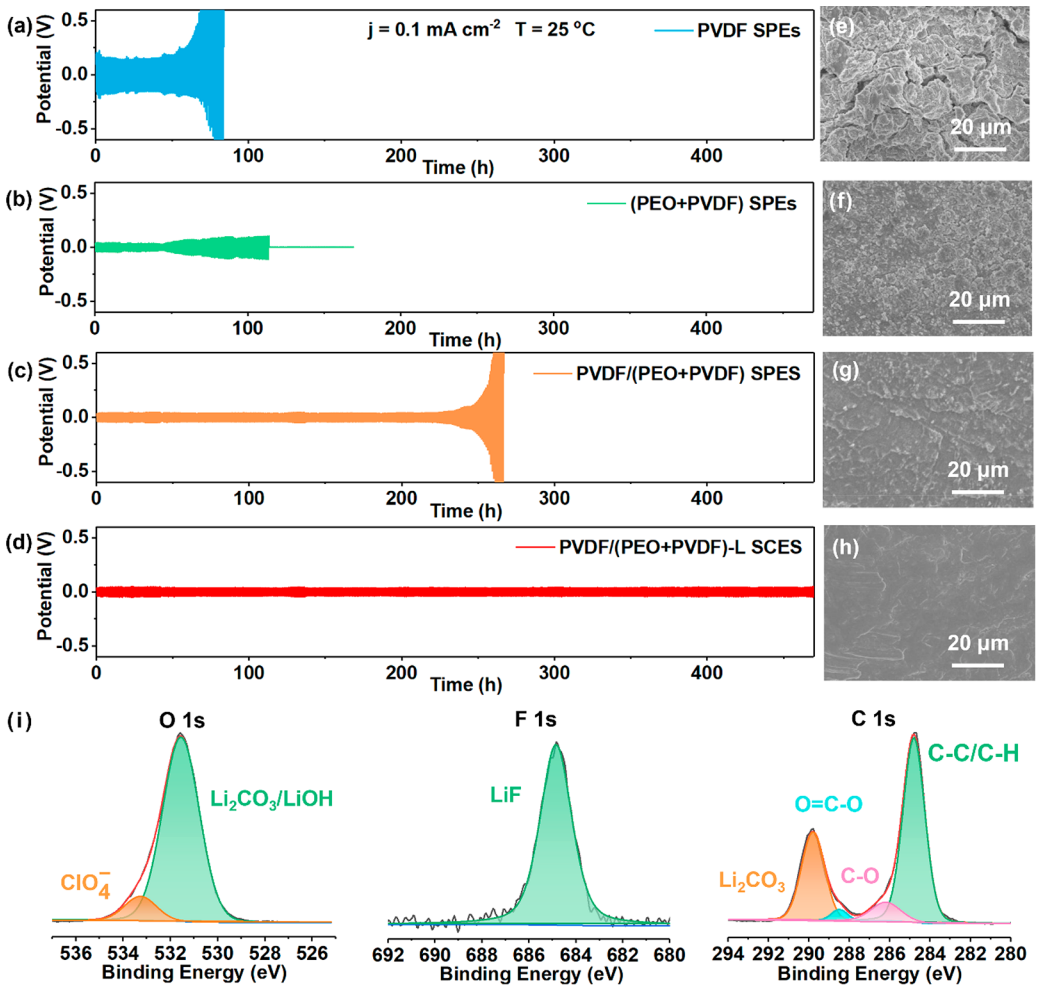

Figure 4. (a–d) Galvanostatic cycling performance for the lithium symmetric cells with a constant current density of 0.1 mA cm^{-2} at 25 °C and (e–h) corresponding surface morphology of the lithium anodes after 50 h cycling. (i) XPS spectra of the lithium anode surface for the Li|PVDF/(PEO+PVDF)-L|Li cell.

(PEO+PVDF)-L SCEs exhibit the overall decreased melting temperature of 106.6 and 145.2 °C, suggesting the reduced crystallinity and enlarged amorphous area introduced by the disruption on the arrangement of polymer chains,[29,38] which will be beneficial for the rapid migration of Li^+ in the polymer matrix resulting in a higher ionic conductivity.[35,38]

The thermal stability of PVDF/(PEO+PVDF)-L SCEs is evaluated through TGA tests (Figure 2c). Consistent with that in the literature,[27,34] the PVDF/(PEO+PVDF)-L SCEs as well as the control groups show a slow and synchronous weight variation in the initial stage and sudden mass loss about at 300 °C, which are mainly attributed to the volatilization of remained DMF plasticizer inside the electrolyte membranes and the accelerated decomposition of polymer matrix caused by the addition of lithium salt, respectively.[27,34] Nevertheless, the thermal decomposition temperature at 300 °C is still enough for the PVDF/(PEO+PVDF)-L SCEs operated in room-temperature LMBs. Furthermore, EA and FT-IR measurements are carried out to separately investigate the content and existing form of the residual DMF solvent. The EA result shows that the calculated mass percentage of remaining DMF is about 20 wt % in all the electrolyte membranes (Table S1). More importantly, this low content of DMF is confirmed to exist as $[Li(DMF)_x]^+$ complexes in the polymer networks but not free molecules, since only the absorption band at 658 cm^{-1} that corresponds the bound DMF appears in the FT-IR spectra (Figure 2d),[39,40] which can strongly illustrates the solid-state characteristics of the PVDF/(PEO+PVDF)-L SCEs.[41]

Electrochemical Properties of PVDF/(PEO+PVDF)-L SCEs. In order to evaluate the effect of the introduction of laponite clay on the Li^+ transfer in PVDF/(PEO+PVDF)-L SCEs, the ionic conductivities of the electrolyte membranes at various temperature are investigated in the temperature range of 25–85 °C (Figures 3a and S2). The filler-free PVDF, (PEO+PVDF), and PVDF/(PEO+PVDF) SPEs which contain equal-content DMF plasticizer for accelerated Li^+ migration,[15,27] all exhibit an acceptable ionic conductivity of about 2.6×10^{-4} S cm^{-1} at room temperature (Figure S2a–c). While, with the incorporation of laponite clay, the PVDF/(PEO+PVDF)-L SCEs can achieve a much improved ionic conductivity of 5.2×10^{-4} S cm^{-1} (Figure S2d), due to the weaker crystallinity and richer amorphous area as confirmed in the XRD and DSC results.[38] Meanwhile, activation energy (E_a) of Li^+ migration inside these electrolyte membranes is calculated by the Arrhenius equation $\sigma(T) = A \exp(-E_a/RT)$. As shown in Figure 3b, the PVDF/(PEO+PVDF)-L SCEs deliver an E_a value of 0.270 eV, which is significantly lower than that of PVDF (0.282 eV), (PEO+PVDF) (0.280 eV), and PVDF/(PEO+PVDF) (0.283 eV) SPEs, revealing the

https://doi.org/10.1021/acsomega.1c05576
ACS Omega 2022, 7, 994–1002

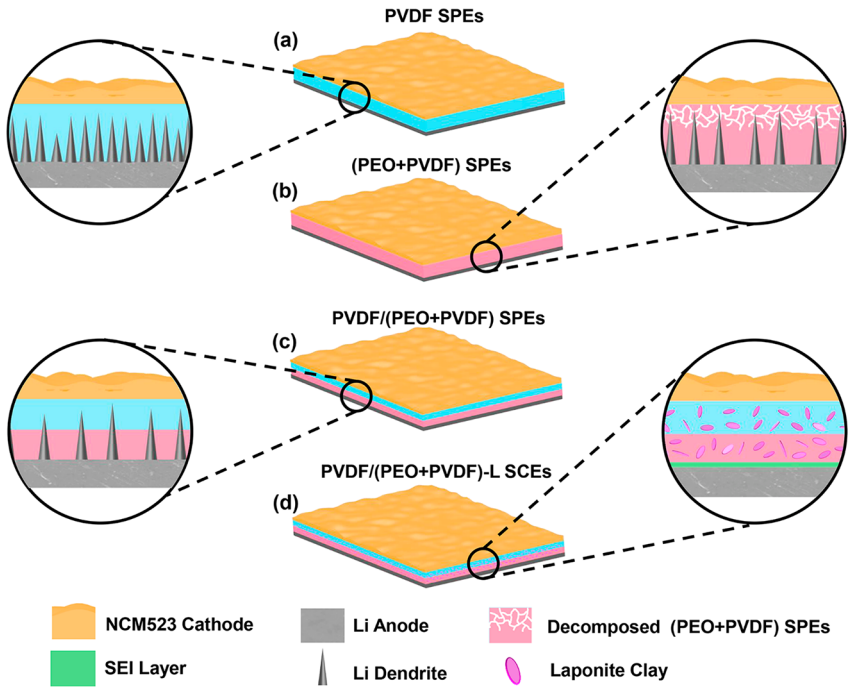

Figure 5. Schematic diagrams for the advantageous performance of PVDF/(PEO+PVDF)-L SCEs relative to the control groups.

easiest ion transfer in the laponite clay-doped polymer networks.[15,32] Moreover, the variation of ionic conductivity depending on the laponite clay content is additionally explored as presented in Figure S3. As expected, the ionic conductivity first increases as the laponite clay content is raised, whereas it decreases because of the nanosheet agglomeration when the mass percentage exceeds 6 wt %.[42] Therefore, the selected amount of 6 wt % here for the laponite clay addition may be quite appropriate to realize an optimal electrochemical performance of PVDF/(PEO+PVDF)-L SCEs.

The electrochemical stability window of SSEs is commonly employed as a crucial indicator to reveal the ability of electrolyte materials to resist decomposition under high voltage.[32,35] It can be found from the LSV curves that the current of (PEO+PVDF) SPEs rises sharply at the voltage of 3.9 V (Figure 3c), representing the initial decomposition occurring on the easily oxidized PEO component.[17,29] Meanwhile, PVDF SPEs exhibit a higher electrochemical stability, and only a slight current fluctuation appears above 4.4 V, due to the existence of strongly electron withdrawing groups (−C−F) in polymer units enabling high voltage maintenance.[31] Therefore, with the PVDF or PVDF-L layer against the cathode to avoid PEO direct exposure under high potential, the double-layer PVDF/(PEO+PVDF) SPEs and PVDF/(PEO+PVDF)-L SCEs both inherit the LSV curve of PVDF SPEs well, displaying a wide electrochemical stability window. This result also suggests that the introduction of laponite clay has no significant effect on the electrochemical stability window of the electrolyte membranes under high voltage.

Furthermore, the calculated values of t_{Li}^{+} according to the EIS combined with DC polarization results shows that the PVDF/(PEO+PVDF)-L SCEs can achieve a t_{Li}^{+} value as high as 0.471 (Figure 3d), which is significantly greater than that of 0.201, 0.227, and 0.195 corresponding to PVDF (Figure S4a), (PEO+PVDF), and PVDF/(PEO+PVDF) SPEs respectively (Figure S4b,c). Such improvement of t_{Li}^{+} for PVDF/(PEO+PVDF)-L SCEs is mainly ascribed to the increased dissociation of lithium salts as well as the hindered transport of ClO_4^- inside the laponite clay-filled polymer networks,[42] and it enables the reduction of the concentration polarization to inhibit the nucleation of lithium dendrites during the charge−discharge process.[28,42]

The interface stability of these electrolyte membranes against the lithium anode during the lithium stripping/plating process is investigated through a galvanostatic polarization measurement on lithium symmetric cells at the current density of 0.1 mA cm^{-2} (Figure 4). Consistent with the literature,[15,33] the PVDF SPEs always show a fairly poor electrochemical stability toward lithium metal, with a sharp voltage increase of the Li|PVDF|Li cell after only cycling for 65 h (Figure 4a). With the introduction of PEO, the blending (PEO+PVDF) SPEs can exhibit a reinforced contact between the electrolyte and lithium anode for decreased interface resistance,[35] which thus delivers a lower initial overpotential and a slightly improved stripping/plating cycling (Figure 4b). However, a short circuit still occurs on the Li|(PEO+PVDF)|Li cell after operation for 115 h, due to the weak mechanical property caused by the soft PEO inside. By comparison, the double-layer PVDF/(PEO+PVDF) SPEs inherit both good mechanical properties and high compatibility with lithium metal and are able to cycle stably for 240 h (Figure 4c). Moreover, owing to the advantage of improved t_{Li}^{+} and enhanced mechanical strength derived from the incorporation of laponite clay (Figure S5), the PVDF/(PEO+PVDF)-L SCEs exhibit an excellent electrochemical stability against lithium metal with dramatically enhanced cycling life of more than 470 h (Figure 4d).

Such a differential lithium plating/stripping process is further illustrated according to the surface morphology of the lithium anode. It is found that the lithium metal has a smooth and dense surface before cycling (Figure S6). As for the lithium symmetric cells cycled for 50 h, the lithium anode against the PVDF SPEs is covered with abundant lithium

https://doi.org/10.1021/acsomega.1c05576
ACS Omega 2022, 7, 994−1002

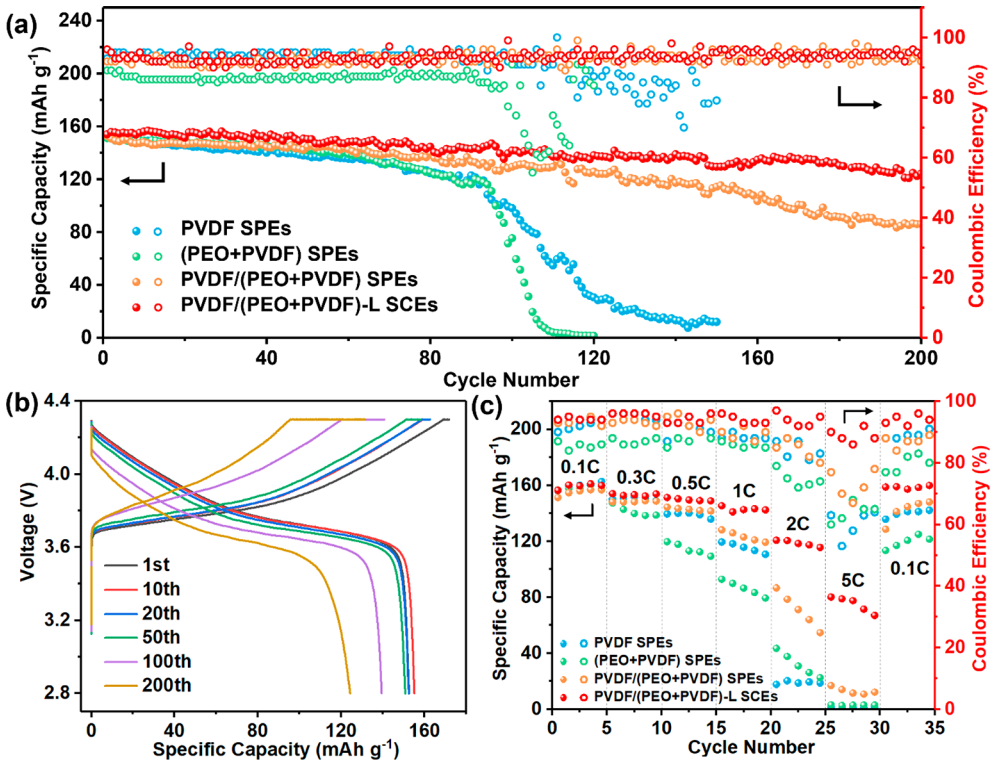

Figure 6. Electrochemical performances of the solid-state LMBs at room temperature. (a) Cycling performance under 0.3 C, (b) corresponding charge−discharge curves of the NCM523|PVDF/(PEO+PVDF)-L|Li cell, and (c) rate capability.

dendrites (Figure 4e), and visible lithium dendrites are also observed on the lithium metal surfaces corresponding to (PEO +PVDF) SPEs and PVDF/(PEO+PVDF) SPEs despite the introduction of PEO (Figure 4f,g), which are considered to be the main reasons for the suddenly sharp rise of cell voltage and even short circuit.[43] In marked contrast to that, the Li|PVDF/(PEO+PVDF)-L|Li cell delivers an uncontaminated lithium anode demonstrating the effective restriction on lithium dendrite formation (Figure 4h), which thus allows a longer period of the stripping/plating cycling as mentioned above. Moreover, XPS analysis of the reaction products on the lithium metal surface shows that abundant Li_2CO_3 (531.5 eV in the O 1s spectra and 289.8 eV in the C 1s spectra),[34,44] LiOH (531.5 eV in the O 1s spectra),[33] and LiF (684.8 eV in the F 1s spectra)[45] can be formed during the lithium plating/stripping process (Figure 4i), which are usually considered to reduce the side reactions between electrolyte and lithium metal for improved electrochemical cycling stability.[34,46]

Mechanism of the Performance Advantages of PVDF/(PEO+PVDF)-L SCEs. According to above analyses, the advantages of the proposed Janus composite structure of PVDF/(PEO+PVDF)-L SCEs are systematically illustrated in Figure 5. When applied to the high-voltage solid-state LMBs, the monolayer PVDF SPEs with a wide electrochemical window are able to withstand the high cathode potential but suffer from a severe lithium dendrite formation caused by the not so good interface contact (Figure 5a); while for the monolayer (PVDF+PEO) SPEs, gradual oxidation and even decomposition usually occur during the charge−discharge process (Figure S7), though the dendrite problem can be moderately improved by the introduced lithium-friendly PEO component (Figure 5b). Constructing a double-layer SPEs membrane with the PVDF layer facing the cathode and the (PEO+PVDF) layer against the lithium anode may endows the electrolyte with both enhanced electrochemical stability under high potential and increased interfacial compatibility to lithium metal, but it is still not enough to achieve a long-term cycling life because the lithium dendrites cannot be completely suppressed (Figure 5c). With the further incorporation of laponite clay nanosheets, the finally obtained PVDF/(PEO +PVDF)-L SCEs not only inherit all the performance advantages of above electrolytes, but also enable the formation of homogeneous SEI film to realize lithium-free anodes on account of the enhanced mechanical property and increased t_{Li^+} (Figure 5d), which is considered essential to realize the excellent cycling performance of high-voltage solid-state LMBs.

Electrochemical Performance of NCM523|PVDF/(PEO +PVDF)-L|Li Cell. Finally, the practical application of PVDF/(PEO+PVDF)-L SCEs in high-voltage solid-state LMBs is evaluated at room temperature using the full CR2032 cells with NCM523 and lithium metal as the cathode and anode, respectively (Figure 6). And as expected, as a result of the mentioned shortcomings of the monolayer electrolyte structure, NCM523|PVDF|Li and NCM523|(PEO+PVDF)|Li cells both show a poor cycling performance with the rapid capacity decay below 100 charge−discharge cycles at the current density of 0.3 C (Figure S8a,b). The cell with double-layer PVDF/(PEO+PVDF) SPEs exhibits a visibly improved cycling life, but its capacity retention rate at the 200th cycle is only about 56.3% (Figure S8c). By comparison, NCM523|PVDF/(PEO+PVDF)-L|Li cell can achieve a highly satisfactory electrochemical performance, with the specific discharge capacity of 153.9 mAh g^{-1} at initial and that of 124.3 mAh g^{-1} after 200 cycles (the capacity retention rate is up to 80.8%) (Figure 6b). Meanwhile, as the current density increases from 0.1 to 5 C, the NCM523|PVDF/(PEO+PVDF)-L|Li cell

https://doi.org/10.1021/acsomega.1c05576
ACS Omega 2022, 7, 994−1002

delivers the always highest specific discharge capacity of 161.1, 153.8, 148.9, 142.4, 115.6, and 80.2 mAh g^{-1} corresponding to 0.1, 0.3, 0.5, 1, 2, and 5 C, respectively (Figures 6c and S9), which will even rise back to 158.7 mAh g^{-1} once the current density returns to 0.1 C, rendering the more excellent rate capability over the others. Besides, the well-matched CV curves from the first to the 30th cycle also demonstrate an outstanding electrochemical stability of PVDF/(PEO +PVDF)-L SCEs (Figure S10).[47]

CONCLUSION

In summary, the double-layer PVDF/(PEO+PVDF)-L SCEs membranes are successfully fabricated by a facile two-step coating process and applied in room-temperature high-voltage LMBs. Among this Janus architecture, the antioxidative PVDF-L layer ensures a good potential tolerance for high-voltage cathode adaptation, whereas the (PEO+PVDF)-L layer in contact with the anode is responsible for providing lithium metal affinity. Especially, the introduction of laponite clay inside not only helps to achieve a high ionic conductivity of 5.2 × 10^{-4} S cm^{-1} at room temperature but also improves the mechanical properties and meanwhile increases the t_{Li}^{+} up to 0.471 for better lithium dendrite suppression. Consequently, the PVDF/(PEO+PVDF)-L SCEs can exhibit a significantly enhanced electrochemical stability against lithium metal with the cycling life over 470 h and deliver the initial discharge capacity as high as 153.9 mAh g^{-1} with the capacity retention up to 80.8% after 200 cycles, when matched with a high-voltage NCM523 electrode and operated at 0.3 C under 25 °C. Such high-performance double-layer SCEs fabricated from the commonly available raw materials are promising for the manufacturing application of solid-state high-voltage LMBs.

EXPERIMENTAL SECTION

Materials. Poly(ethylene oxide) (PEO, average M_w = 600000) and lithium perchlorate ($LiClO_4$, 99.99%) were purchased from Aladdin. Poly(vinylidene fluoride) (PVDF, average M_w = 1 000 000) was bought from Shenzhen Kejingstar Technology Ltd. *N*,*N*-Dimethylformamide (DMF, Sinopharm) was used for the preparation of electrolyte slurry. Laponite clay (XLG: $Mg_{5.34}Li_{0.66}Si_8O_{20}(OH)Na_{0.66}$, BYK) was employed as the inorganic nanofiller. Commercial $LiNi_{0.5}Co_{0.2}Mn_{0.3}O_2$ (NCM523) purchased from Tianjin B&M Science and Technology Joint-Stock Co., Ltd., was used as the high-voltage cathode material. *N*-methylpyrrolidone (NMP) and acetylene black (Sinopharm) were used for the preparation of cathode slurry. Al foils and lithium sheets were both bought from China Energy Lithium Co., Ltd.

Preparation of Double-Layer PVDF/(PEO+PVDF)-L SCEs. The double-layer PVDF/(PEO+PVDF)-L SCEs were typically prepared by a layer-by-layer coating technology (Figure S1). First, laponite clay powder (6 wt % relative to the polymer matrix, 0.054 g) was dispersed in DMF (8.2 mL) by ultrasonic treatment for 15 min to form a uniform dispersion. PVDF (0.9 g) and $LiClO_4$ (0.3 g) was then added into the mixture with stirring at 45 °C for 4 h to obtain the PVDF-L slurry. Meanwhile, the (PVDF+PEO)-L slurry was prepared through the same procedure but replacing the PVDF component with the combination of PVDF (0.45 g) and PEO (0.45 g). After that, the as-obtained PVDF-L slurry was coated on a clean glass plate by a film applicator (Figure S1a, b) and dried at 60 °C for 30 min to form single-layer PVDF-L membranes (Figure S1c), whose thickness was controlled to about 50 μm. And, a second coating using the (PVDF+PEO)-L slurry was subsequently applied directly on the above predried PVDF-L membranes (Figure S 1d,e). Finally, the double-layer PVDF/(PEO+PVDF)-L SCEs of about 100 μm total thickness could be obtained by another drying treatment under vacuum at 60 °C for 24 h (Figure S 1f).

Preparation of PVDF SPEs, (PEO+PVDF) SPEs, and Double-Layer PVDF/(PEO+PVDF) SPEs. For comparison, PVDF and (PEO+PVDF) SPEs were fabricated by a single-layer coating process with the drying treatment under vacuum at 60 °C for 24 h, and the double-layer PVDF/(PEO+PVDF) SPEs were prepared in the same way as PVDF/(PEO+PVDF)-L SCEs, but without the addition of laponite clay.

Material Characterizations. The microstructures of the as-prepared electrolyte membranes were observed by a field emission scanning electron microscopy (FESEM, Hitachi SU8020). The attached energy dispersive spectrometer (EDS, Horiba Scientific) was used for the element distribution characterization. X-ray diffraction (XRD, Rigaku D/MAX2500VL/PC) with a Cu−Kα radiation (λ = 1.5405 Å) was employed to analyze the crystal structure at 40 kV and 80 mA in the 2θ range of 10−80°. Differential scanning calorimetry (DSC) measurements were carried out on a DSC instrument (Netzsch, DSC214) with the heating rate of 5 °C min^{-1} from 30 to 300 °C under an N_2 atmosphere to explore the phase transition behavior. The thermal stability was evaluated by a thermogravimetric analysis instrument (TGA, Netzsch, STA449F5) from 30 to 600 °C with the heating rate of 10 °C min^{-1} under an N_2 atmosphere. The content of the remaining DMF in electrolyte membranes was determined accurately by elemental analysis (EA). The mechanical properties were investigated by an electronic tensile tester (Instron 5965) with the stretching rate of 100 mm min^{-1}. The chemical composition was characterized by Fourier-transform infrared spectrometry (FT-IR, Thermo Nicolet, iS10) from 400 to 4000 cm^{-1}. X-ray photoelectron spectroscopy (XPS, Thermo, ESCALAB 250Xi) was employed for the composition analysis of the lithium anode interface.

Electrochemical Measurements. The ionic conductivities of electrolyte membranes were investigated by AC impedance spectroscopy measurements performed on the assembled stainless steel (SS)|SSEs|SS cells, using a CHI660e electrochemical workstation (Shanghai Chenhua Instrument, China). The conductivity value could be calculated by the following equation:

$$\sigma = \frac{l}{R \cdot S}$$

in which R, l, and S separately represented the bulk resistance, thickness, and area of the electrolyte membranes. Linear sweep voltammetry (LSV) measurements on SS|SSEs|Li cells were performed to evaluate the electrochemical stability window within the voltage range of 2−6 V at a scan rate of 5 mV s^{-1}. t_{Li}^{+} was obtained by the combined electrochemical impedance spectroscopy (EIS) and direct current (DC) polarization method, which could be calculated according to the equation:

$$t_{Li^+} = \frac{I_S(\Delta V - I_0 R_0)}{I_0(\Delta V - I_S R_S)}$$

where ΔV was the applied DC voltage, I_0 and R_0 indicated the initial current and interfacial resistance respectively, I_S and R_S

https://doi.org/10.1021/acsomega.1c05576
ACS Omega 2022, 7, 994−1002

separately represented the steady-state current and interfacial resistance. To investigate the lithium stripping/plating behavior, the galvanostatic polarization tests on symmetric Li|SSEs|Li cells were carried out at a current density of 0.1 mA cm^{-2} at 25 °C.

For the preparation of NCM523 electrodes, commercial NCM523, PVDF, and acetylene black were mixed at a mass ratio of 8:1:1 in appropriate amount of NMP with magnetic stirring for 12 h, and the resultant slurry was then coated on Al foil and finally dried at 70 °C for 8 h in air to obtain the cathode foil. The full cells (CR2032) were assembled with an NCM523 cathode (12 mm), SSEs (16 mm), and lithium anode (15.6 mm) in an Ar-filled glovebox (O_2 < 0.5 ppm, H_2O < 0.5 ppm) and tested on a multichannel battery tester (Neware Battery Testing System, Shenzhen Neware Electronic, China) over the voltage range of 2.8−4.3 V under 0.3 C at 25 °C.

■ ASSOCIATED CONTENT

Supporting Information

The Supporting Information is available free of charge at https://pubs.acs.org/doi/10.1021/acsomega.1c05576.

Schematic diagram for the fabrication of double-layer PVDF/(PEO+PVDF)-L SCEs membranes. EIS performed on the assembled symmetric SS|SSEs|SS cells. Ionic conductivity of the PVDF/(PEO+PVDF)-L SCEs depending on the content of laponite clay added. DC polarization curves for the Li symmetrical cells of control groups. Stress−strain curves of the as-prepared electrolyte membranes. Surface morphology of fresh lithium anode. CV curves of NCM523|(PEO+PVDF)|Li cells at 2 mV s^{-1}. The charge−discharge curves of the control cells at 0.3 C under 25 °C. The charge−discharge curves of the NCM523|PVDF/(PEO+PVDF)-L|Li cell at different current densities under 25 °C. CV curves of NCM523|PVDF/(PEO+PVDF)-L|Li cells at 2 mV s^{-1}. EA results of the as-prepared electrolyte membranes (PDF)

■ AUTHOR INFORMATION

Corresponding Authors

Kun Shi − *School of Chemistry and Chemical Engineering, Hefei University of Technology, Hefei, Anhui 230009, China; Institute of Energy, Hefei Comprehensive National Science Center, Hefei, Anhui 230031, China*; Email: shikun@hfut.edu.cn

Weixin Zhang − *School of Chemistry and Chemical Engineering, Hefei University of Technology, Hefei, Anhui 230009, China; Institute of Energy, Hefei Comprehensive National Science Center, Hefei, Anhui 230031, China*; orcid.org/0000-0001-6979-8901; Email: wxzhang@hfut.edu.cn

Authors

Lei Zou − *School of Chemistry and Chemical Engineering, Hefei University of Technology, Hefei, Anhui 230009, China*

Zhengjie Xu − *School of Chemistry and Chemical Engineering, Hefei University of Technology, Hefei, Anhui 230009, China*

Zeheng Yang − *School of Chemistry and Chemical Engineering, Hefei University of Technology, Hefei, Anhui 230009, China*

Complete contact information is available at: https://pubs.acs.org/10.1021/acsomega.1c05576

Notes

The authors declare no competing financial interest.

■ ACKNOWLEDGMENTS

The authors gratefully acknowledge the support from the National Natural Science Foundation of China (NSFC Grants 21908037, 91834301) and the Fundamental Research Funds for the Central Universities (JZ2021HGTB0119).

■ REFERENCES

(1) Ye, L. H.; Li, X. A dynamic stability design strategy for lithium metal solid state batteries. *Nature* **2021**, *593*, 218−222.

(2) Albertus, P.; Babinec, S.; Litzelman, S.; Newman, A. Status and challenges in enabling the lithium metal electrode for high-energy and low-cost rechargeable batteries. *Nat. Energy* **2018**, *3*, 16−21.

(3) Kim, K. J.; Balaish, M.; Wadaguchi, M.; Kong, L. P.; Rupp, J. L. M. Solid-state Li-metal batteries: Challenges and horizons of oxide and sulfide solid electrolytes and their interfaces. *Adv. Energy Mater.* **2021**, *11*, 2002689.

(4) Zuo, T. T.; Shi, Y.; Wu, X. W.; Wang, P. F.; Wang, S. H.; Yin, Y. X.; Wang, W. P.; Ma, Q.; Zeng, X. X.; Ye, H.; Wen, R.; Guo, Y. G. Constructing a stable lithium metal-gel electrolyte interface for quasi-solid-state lithium batteries. *ACS Appl. Mater. Interfaces* **2018**, *10*, 30065−30070.

(5) Um, J. H.; Yu, S. H. Unraveling the mechanisms of lithium metal plating/stripping via in situ/operando analytical techniques. *Adv. Energy Mater.* **2021**, *11*, 2003004.

(6) Wu, H. P.; Jia, H.; Wang, C. M.; Zhang, J. G.; Xu, W. Recent progress in understanding solid electrolyte interphase on lithium metal anodes. *Adv. Energy Mater.* **2021**, *11*, 2003092.

(7) Zhang, X. Y.; Wang, A. X.; Liu, X. J.; Luo, J. Y. Dendrites in lithium metal anodes: Suppression, regulation, and elimination. *Acc. Chem. Res.* **2019**, *52*, 3223−3232.

(8) Chen, H.; Zhou, C. J.; Dong, X. R.; Yan, M.; Liang, J. Y.; Xin, S.; Wu, X. W.; Guo, Y. G.; Zeng, X. X. Revealing the superiority of fast ion conductor in composite electrolyte for dendrite-free lithium-metal batteries. *ACS Appl. Mater. Interfaces* **2021**, *13*, 22978−22986.

(9) Wang, L.; Zhou, Z. Y.; Yan, X.; Hou, F.; Wen, L.; Luo, W. B.; Liang, J.; Dou, S. X. Engineering of lithium-metal anodes towards a safe and stable battery. *Energy Storage Mater.* **2018**, *14*, 22−48.

(10) Tu, Z. Y.; Choudhury, S.; Zachman, M. J.; Wei, S. Y.; Zhang, K. H.; Kourkoutis, L. F.; Archer, L. A. Designing artificial solid-electrolyte interphases for single-ion and high-efficiency transport in batteries. *Joule* **2017**, *1*, 394−406.

(11) Peng, Z.; Zhao, N.; Zhang, Z. G.; Wan, H.; Lin, H.; Liu, M.; Shen, C.; He, H. Y.; Guo, X. X.; Zhang, J. G.; Wang, D. Y. Stabilizing Li/electrolyte interface with a transplantable protective layer based on nanoscale LiF domains. *Nano Energy* **2017**, *39*, 662−672.

(12) Zheng, J. M.; Engelhard, M. H.; Mei, D. H.; Jiao, S. H.; Polzin, B. J.; Zhang, J. G.; Xu, W. Electrolyte additive enabled fast charging and stable cycling lithium metal batteries. *Nat. Energy* **2017**, *2*, 17012.

(13) Cheng, X. B.; Zhao, M. Q.; Chen, C.; Pentecost, A.; Maleski, K.; Mathis, T.; Zhang, X. Q.; Zhang, Q.; Jiang, J. J.; Gogotsi, Y. Nanodiamonds suppress the growth of lithium dendrites. *Nat. Commun.* **2017**, *8*, 336−344.

(14) Zhang, X. Q.; Cheng, X. B.; Chen, X.; Yan, C.; Zhang, Q. Fluoroethylene carbonate additives to render uniform Li deposits in lithium metal batteries. *Adv. Funct. Mater.* **2017**, *27*, 1605989.

(15) Shi, K.; Xu, Z. J.; Huang, M. Q.; Zou, L.; Zheng, D. W.; Yang, Z. H.; Zhang, W. X. Solid-state polymer electrolytes with polypropylene separator-reinforced sandwich structure for room-temperature lithium ion batteries. *J. Membr. Sci.* **2021**, *638*, 119713.

(16) Manthiram, A.; Yu, X. W.; Wang, S. F. Lithium battery chemistries enabled by solid-state electrolytes. *Nat. Rev. Mater.* **2017**, *2*, 16103.

(17) Liu, K.; Zhang, R. H.; Sun, J.; Wu, M. C.; Zhao, T. S. Polyoxyethylene (PEO)|PEO-perovskite|PEO composite electrolyte for all-solid-state lithium metal batteries. *ACS Appl. Mater. Interfaces* **2019**, *11*, 46930−46937.
(18) Xue, P.; Liu, S. R.; Shi, X. L.; Sun, C.; Lai, C.; Zhou, Y.; Sui, D.; Chen, Y.; Liang, J. J. A hierarchical silver-nanowire-graphene host enabling ultrahigh rates and superior long-term cycling of lithium-metal composite anodes. *Adv. Mater.* **2018**, *30*, 1804165.
(19) Shi, Y. J.; Wang, Z. B.; Gao, H.; Niu, J. Z.; Ma, W. S.; Qin, J. Y.; Peng, Z. Q.; Zhang, Z. H. A self-supported, three-dimensional porous copper film as a current collector for advanced lithium metal batteries. *J. Mater. Chem. A* **2019**, *7*, 1092−1098.
(20) Ji, X.; Hou, S.; Wang, P. F.; He, X. Z.; Piao, N.; Chen, J.; Fan, X. L.; Wang, C. S. Solid-state electrolyte design for lithium dendrite suppression. *Adv. Mater.* **2020**, *32*, 2002741.
(21) Wen, K. H.; Tan, X.; Chen, T. H.; Chen, S. M.; Zhang, S. J. Fast Li-ion transport and uniform Li-ion flux enabled by a double-layered polymer electrolyte for high performance Li metal battery. *Energy Storage Mater.* **2020**, *32*, 55−64.
(22) Famprikis, T.; Canepa, P.; Dawson, J. A.; Islam, M. S.; Masquelier, C. Fundamentals of inorganic solid-state electrolytes for batteries. *Nat. Mater.* **2019**, *18*, 1278−1291.
(23) Zhang, S. Z.; Liang, T. B.; Wang, D. H.; Xu, Y. J.; Cui, Y. L.; Li, J. R.; Wang, X. L.; Xia, X. H.; Gu, C. D.; Tu, J. P. A stretchable and safe polymer electrolyte with a protecting-layer strategy for solid-state lithium metal batteries. *Adv. Sci.* **2021**, *8*, 2003241.
(24) Zhou, Q.; Ma, J.; Dong, S. M.; Li, X. F.; Cui, G. L. Intermolecular chemistry in solid polymer electrolytes for high-energy-density lithium batteries. *Adv. Mater.* **2019**, *31*, 1902029.
(25) Li, M.; Wang, C. S.; Chen, Z. W.; Xu, K.; Lu, J. New concepts in electrolytes. *Chem. Rev.* **2020**, *120*, 6783−6819.
(26) Xu, B. Y.; Li, X. Y.; Yang, C.; Li, Y. T.; Grundish, N. S.; Chien, P. H.; Dong, K.; Manke, I.; Fang, R. Y.; Wu, N.; Xu, H. H.; Dolocan, A.; Goodenough, J. B. Interfacial chemistry enables stable cycling of all-solid-state Li metal batteries at high current densities. *J. Am. Chem. Soc.* **2021**, *143*, 6542−6550.
(27) Yao, P. C.; Zhu, B.; Zhai, H. W.; Liao, X. B.; Zhu, Y. X.; Xu, W. H.; Cheng, Q.; Jayyosi, C.; Li, Z.; Zhu, J.; Myers, K. M.; Chen, X.; Yang, Y. PVDF/palygorskite nanowire composite electrolyte for 4 V rechargeable lithium batteries with high energy density. *Nano Lett.* **2018**, *18*, 6113−6120.
(28) Liang, J. Y.; Zeng, X. X.; Zhang, X. D.; Zuo, T. T.; Yan, M.; Yin, Y. X.; Shi, J. L.; Wu, X. W.; Guo, Y. G.; Wan, L. J. Engineering janus interfaces of ceramic electrolyte via distinct functional polymers for stable high-voltage Li-metal batteries. *J. Am. Chem. Soc.* **2019**, *141*, 9165−9169.
(29) Chen, L.; Li, Y. T.; Li, S. P.; Fan, L. Z.; Nan, C. W.; Goodenough, J. B. PEO/garnet composite electrolytes for solid-state lithium batteries: From "ceramic-in-polymer" to "polymer-in-ceramic. *Nano Energy* **2018**, *46*, 176−184.
(30) Zhou, W. D.; Wang, Z. W.; Pu, Y.; Li, Y. T.; Xin, S.; Li, X. F.; Chen, J. F.; Goodenough, J. B. Double-layer polymer electrolyte for high-voltage all-solid-state rechargeable batteries. *Adv. Mater.* **2019**, *31*, 1805574.
(31) Mohamed, N. S.; Arof, A. K. Investigation of electrical and electrochemical properties of PVDF-based polymer electrolytes. *J. Power Sources* **2004**, *132*, 229−234.
(32) Yu, X. R.; Wang, L. L.; Ma, J.; Sun, X. W.; Zhou, X. H.; Cui, G. L. Selectively wetted rigid-flexible coupling polymer electrolyte enabling superior stability and compatibility of high-voltage lithium metal batteries. *Adv. Energy Mater.* **2020**, *10*, 1903939.
(33) Sun, J. Q.; Yao, X. M.; Li, Y. G.; Zhang, Q. H.; Hou, C. Y.; Shi, Q. W.; Wang, H. Z. Facilitating interfacial stability via bilayer heterostructure solid electrolyte toward high-energy, safe and adaptable lithium batteries. *Adv. Energy Mater.* **2020**, *10*, 2000709.
(34) Liu, W. Y.; Yi, C. J.; Li, L. P.; Liu, S. L.; Gui, Q. Y.; Ba, D. L.; Li, Y. Y.; Peng, D. L.; Liu, J. P. Designing polymer-in-salt electrolyte and fully infiltrated 3D electrode for integrated solid-state lithium batteries. *Angew. Chem., Int. Ed.* **2021**, *60*, 12931−12940.
(35) Xie, Z. K.; Wu, Z. J.; An, X. W.; Yue, X. Y.; Xiaokaiti, P.; Yoshida, A.; Abudula, A.; Guan, G. Q. A sandwich-type composite polymer electrolyte for all-solid-state lithium metal batteries with high areal capacity and cycling stability. *J. Membr. Sci.* **2020**, *596*, 117739.
(36) Wang, H.; Lin, C.; Yan, X. H.; Wu, A. M.; Shen, S. Y.; Wei, G. H.; Zhang, J. L. Mechanical property-reinforced PEO/PVDF/$LiClO_4$/SN blend all solid polymer electrolyte for lithium ion batteries. *J. Electroanal. Chem.* **2020**, *869*, 114156.
(37) Song, X. F.; Zhang, Y. N.; Ye, Y. W.; Liu, Z. F.; Cheng, F.; Li, H. R. A durable gel polymer electrolyte with excellent cycling and rate performance for enhanced lithium storage. *ACS Appl. Energy Mater.* **2020**, *3*, 4906−4913.
(38) Huo, H. Y.; Chen, Y.; Luo, J.; Yang, X. F.; Guo, X. X.; Sun, X. L. Rational design of hierarchical "ceramic-in-polymer" and "polymer-in-ceramic" electrolytes for dendrite-free solid-state batteries. *Adv. Energy Mater.* **2019**, *9*, 1804004.
(39) Zhang, X.; Han, J.; Niu, X. F.; Xin, C. Z.; Xue, C. J.; Wang, S.; Shen, Y.; Zhang, L.; Li, L. L.; Nan, C. W. High cycling stability for solid-state Li metal batteries via regulating solvation effect in poly(vinylidene fluoride)-based electrolytes. *Batteries Supercaps* **2020**, *3*, 876−883.
(40) Fujii, K.; Wakamatsu, H.; Todorov, Y.; Yoshimoto, N.; Morita, M. Structural and electrochemical properties of Li ion solvation complexes in the salt-concentrated electrolytes using an aprotic donor solvent, N,N-dimethylformamide. *J. Phys. Chem. C* **2016**, *120*, 17196−17204.
(41) Zhang, X.; Wang, S.; Xue, C. J.; Xin, C. Z.; Lin, Y. H.; Shen, Y.; Li, L. L.; Nan, C. W. Response to comment on "Self-suppression of lithium dendrite in all-solid-state lithium metal batteries with poly(vinylidene difluoride)-based solid electrolytes. *Adv. Mater.* **2020**, *32*, 2000026.
(42) Chen, L.; Li, W. X.; Fan, L. Z.; Nan, C. W.; Zhang, Q. Intercalated electrolyte with high transference number for dendrite-free solid-state lithium batteries. *Adv. Funct. Mater.* **2019**, *29*, 1901047.
(43) Wan, J. Y.; Xie, J.; Kong, X.; Liu, Z.; Liu, K.; Shi, F. F.; Pei, A.; Chen, H.; Chen, W.; Chen, J.; Zhang, X. K.; Zong, L. Q.; Wang, J. Y.; Chen, L. Q.; Qin, J.; Cui, Y. Ultrathin, flexible, solid polymer composite electrolyte enabled with aligned nanoporous host for lithium batteries. *Nat. Nanotechnol.* **2019**, *14*, 705−712.
(44) Zhang, S. M.; Yang, G. J.; Liu, S.; Li, X. Y.; Wang, X. F.; Wang, Z. X.; Chen, L. Q. Understanding the dropping of lithium plating potential in carbonate electrolyte. *Nano Energy* **2020**, *70*, 104486.
(45) Lu, H. L.; Xu, N.; Ni, X. Y.; Zhou, J. Q.; Liu, J.; Wang, Z. K.; Qian, T.; Yan, C. L. Functional-selected LiF-intercalated-graphene enabling ultra-stable lithium sulfur battery. *J. Energy Chem.* **2021**, *58*, 78−84.
(46) Yu, J.; Lyu, Y. Q.; Liu, J. P.; Effat, M. B.; Kwok, S. C. T.; Wu, J. X.; Ciucci, F. Enabling non-flammable Li-metal batteries via electrolyte functionalization and interface engineering. *J. Mater. Chem. A* **2019**, *7*, 17995−18002.
(47) Jin, Y. M.; Liu, C. J.; Zong, X.; Li, D.; Fu, M. Y.; Tan, S. P.; Xiong, Y. P.; Wei, J. H. Interface engineering of $Li_{1.3}Al_{0.3}Ti_{1.7}(PO_4)_3$ ceramic electrolyte via multifunctional interfacial layer for all-solid-state lithium batteries. *J. Power Sources* **2020**, *460*, 228125−228133.

https://doi.org/10.1021/acsomega.1c05576
ACS Omega 2022, 7, 994−1002